Food Innovation and Advances

ARTICLE

Open Access

https://doi.org/10.48130/fia-0026-0023

Food Innovation and Advances **2026**, 5(2): 287–302

Blueberry derived exosome like nanoparticles alleviate CCl_4 induced acute liver injury by inhibiting ACSL4–ALOX15 mediated ferroptosis

Ruolan Liu[1], Feng Zhang[1], Chuanhai Zhang[2], Tongxiao Xu[1], Teng Wang[1], Yanan Wang[1], Ying Ding[1], Kunlun Huang[1,3] and Xiaoyun He[1,3*]

[1] *Key Laboratory of Precision Nutrition and Food Quality, College of Food Science and Nutritional Engineering; China Agricultural University, Beijing 100083, China*
[2] *Department of Physiology, UT Southwestern Medical Center, Dallas, TX 75390, USA*
[3] *Key Laboratory of Safety Assessment of Genetically Modified Organism (Food Safety), Ministry of Agriculture and Rural Affairs of the P.R. China, Beijing 100083, China*
* Correspondence: hexiaoyun@cau.edu.cn (He X)

Abstract

Blueberry (*Vaccinium* spp.), a flowering plant in the family Ericaceae, is rich in bioactive compounds such as polyphenols, anthocyanins, and flavonoids, which exhibit anti-inflammatory, antioxidant, and anticancer properties. Increasing evidence suggests that plant-derived exosome-like nanoparticles (PELNs) possess diverse therapeutic activities and hold promise for improving liver function. Acute liver injury (ALI) is a clinical syndrome for which effective pharmacological interventions remain limited. The present study aimed to investigate whether orally administered blueberry-derived exosome-like nanoparticles (BELNs) can ameliorate ALI and to elucidate the underlying mechanisms. Both *in vivo* and *in vitro* experiments demonstrated that BELNs significantly attenuated CCl_4-induced ALI. Specifically, BELNs reduced oxidative stress and inhibited the accumulation of lipid peroxidation products. Mechanistic analyses revealed that BELNs alleviated lipid peroxidation and ferroptosis by suppressing the ACSL4–ALOX15 signaling pathway, specifically reducing its expression by approximately 70% ($p < 0.001$) and thereby protecting hepatocytes from injury. Further investigation identified procyanidin B2 (PCB2) as one of the key active components in BELNs responsible for their antioxidant effects. In summary, this study provides new insights into the therapeutic potential of blueberries and their derived natural products and establishes a mechanistic basis for the clinical translation of PELNs.

Citation: Liu R, Zhang F, Zhang C, Xu T, Wang T, et al. 2026. Blueberry derived exosome like nanoparticles alleviate CCl_4 induced acute liver injury by inhibiting ACSL4–ALOX15 mediated ferroptosis. *Food Innovation and Advances* 5(2): 287–302 https://doi.org/10.48130/fia-0026-0023

Introduction

Blueberries (*Vaccinium* spp.) are classified among the five major health-promoting foods for human consumption. They are recognized as the 'king of the fruit world'[1]. Blueberries originated in Eastern North America and high-latitude cold regions, with a history dating back thousands of years. The vast majority of blueberry cultivars cultivated in China were introduced from abroad. The major blueberry varieties were highbush (*Vaccinium corymbosum*), half-highbush (*Vaccinium corymbosum* × *Vaccinium angustifolium*), rabbit-eye (*Vaccinium virgatum*), and lowbush (*Vaccinium angustifolium*)[2]. Blueberry fruits are valued for their palatable flavor profile and diverse bioactive constituents[3]. However, postharvest blueberries exhibit high perishability. This is due to susceptibility to physical injury and microbial spoilage. Such factors lead to limited storage duration and substantial economic wastage[4]. Given the seasonal nature and limited shelf life of fresh blueberries, processed derivatives have gained popularity as functional food products, such as juices, wines, vinegars, jams, dried fruits, and powdered concentrates[5]. While innovative functional food products generate considerable market attention, significant challenges persist. These challenges include bioactive compound bioavailability, formulation compatibility, stability maintenance, and quality assurance compliance with global food safety regulations. Therefore, researchers can detect and extract the active components in blueberries to maximize their nutritional value.

Blueberries are abundant in flavonoids, particularly diverse anthocyanins. Anthocyanins constitute over 50% of the total polyphenolic content present in blueberries[6]. These bioactive compounds confer a range of physiological benefits. They exhibit potent antioxidant, anti-inflammatory, and antitumor activities, alongside the capacity to enhance metabolic health and cognitive function[7]. Research has demonstrated that blueberry polyphenols can mitigate alcohol-induced hepatic steatosis in C57BL/6J mice[8]. Additionally, supplementation with blueberry juice has been shown to attenuate CCl_4-induced liver fibrosis[9]. PCB2, the most abundant proanthocyanidin in blueberries, exhibits a spectrum of biological activities, including notable hepatoprotective effects. It has been demonstrated to ameliorate pathological alterations in CCl_4-induced murine liver fibrosis[10]. Notably, blueberries contain bioactive molecules. Beyond these, natural nanostructures known as blueberry-derived exosome-like nanoparticles (BELNs) are increasingly recognized as a valuable resource. They contribute to the development of human health and novel biotherapeutics.

PELNs can be isolated from various fresh vegetables and fruit juices, such as grape[11], grapefruit[12], ginger[13], lemon[14], and so on. PELNs are nanoscale membrane vesicles isolated from various plants, encapsulating diverse bioactive constituents including lipids, proteins, and nucleic acids. These molecular constituents play pivotal roles in regulating fundamental physiological processes in plants, such as growth and development, immune defense, and tissue regeneration. In contrast to synthetic nanoparticles and mammalian cell-derived exosomes (MDEs), PELNs exhibit reduced toxicity, lower immunogenicity, and superior biocompatibility. These intrinsic characteristics provide a solid basis for their clinical translation across a diverse spectrum of pathological conditions. Notably, PELNs exhibit inherent biological targeting capabilities. They enable efficient drug loading and site-specific delivery to particular tissues.

Therefore, they present a promising platform for advancing novel drug delivery systems (DDS)[15]. Numerous studies have explored blueberries and their component PCB2. However, the role of BELNs in liver injury models remains poorly understood. Research on their involvement in ferroptosis regulation is also lacking. Additionally, the contribution of specific bioactive compounds within PELNs is unclear. The contribution of specific bioactive compounds within BELNs, such as PCB2, has not been previously elucidated. Furthermore, the specific molecular pathways and mechanisms through which BELNs and PCB2 confer their hepatoprotective effects require systematic investigation. Our research filled the gaps in these theories.

ALI is a prevalent and severe clinical entity. It is characterized by the sudden onset of hepatic dysfunction in people without pre-existing liver conditions. Diverse etiological factors often precipitate this, and there is a significant risk of rapid progression to acute liver failure (ALF)[16]. Its clinical presentation predominantly includes jaundice, coagulopathy, and hepatic encephalopathy. Ferroptosis driven by lipid peroxidation is the key underlying mechanism of hepatocellular damage. Failure to intervene in a timely and effective manner, the condition can advance through stages of liver fibrosis, liver failure, cirrhosis, and hepatocellular carcinoma, frequently culminating in mortality[17]. In recent years, propelled by factors such as pharmaceutical misuse, adverse lifestyle choices, and environmental pollutants, the global incidence of ALI has shown a marked upward trend, establishing it as a pressing public health concern worldwide. Liver transplantation remains the most effective therapeutic intervention for end-stage liver disease in clinical practice. Its implementation is, however, severely limited by the limited availability of donor organs[18]. Under these circumstances, there is an urgent need to investigate novel therapeutic strategies for liver injury to effectively prevent and mitigate its initiation and progression. CCl_4, a classical hepatotoxic agent, is widely employed in experimental settings, and the CCl_4-induced ALI model represents one of the most extensively utilized preclinical systems[19,20]. This study aims to elucidate the pathogenic mechanisms underlying ALI using a CCl_4-induced murine model and to investigate potential therapeutic interventions.

Accordingly, this study aims to study the role of BELNs in ameliorating CCl_4-induced ALI. BELNs were isolated from blueberry juice via ultracentrifugation and systematically characterized for their physicochemical properties. The therapeutic efficacy of orally administered BELNs was assessed in a mouse model of ALI; we particularly focus on their modulatory effects on lipid peroxidation and the ferroptosis pathway. In addition, the cellular uptake efficiency of BELNs by AML12 hepatocytes was evaluated *in vitro*. Their therapeutic efficacy against CCl_4-induced damage was systematically validated at both phenotypic and molecular levels. Finally, PCB2, a relatively abundant active component, was isolated from BELNs. We evaluated its capacity to ameliorate ALI *in vitro* and compared its therapeutic performance with that of the whole BELNs. Collectively, these observations offer new perspectives for the clinical translation of PELNs. They also propose a potential treatment approach for ALI management.

Materials and methods

Isolation and purification of BELNs

BELNs were isolated from fresh blueberries (Yunnan Province, China) belonging to the southern highbush variety 'Eureka'. After washing with distilled water, blueberries were homogenized using a juicer to obtain crude juice. The juice was subsequently subjected to sequential centrifugation at 3,000 × g for 10 min, 5,000 × g for 20 min, and 10,000 × g for 60 min at 4 °C to remove dead cells, cellular debris, and large particles, respectively. The resulting supernatant was subjected to ultracentrifugation at 150,000 × g for 2 h (Beckman Coulter, USA)[21]. Following the initial ultracentrifugation, the pellet was resuspended in ice-cold PBS and centrifuged again at 150,000 × g for 1 h. The final pellet was resuspended in 500 μL of PBS and filtered through 0.22 μm membranes. The purified BELNs were aliquoted and stored at −80 °C for subsequent analysis. The protein concentration of BELNs was determined using a BCA assay kit (P0010, Beyotime Biotechnology, China).

Identification and characterization of BELNs

The zeta potential and hydrodynamic diameter of BELNs were measured by Nano-ZS90 Nanosizer (Malvern Instruments Ltd., UK). Particle size concentration and distribution were determined with a NanoSight LM10 system. Samples were appropriately diluted 1:100 in PBS (1×) and measured in triplicate with 60-s video captures at a detection threshold of 3. Nanoparticle morphology was characterized by transmission electron microscopy (TEM, Hitachi, Japan). Briefly, a sample of 5 μL was placed on a carbon-coated copper grid, air-dried, and subsequently imaged using TEM[22].

Lipidomic analysis of BELNs

Lipids were extracted from BELNs using a methyl tert-butyl ether/methanol/water system. The organic phase was collected, dried, reconstituted in isopropanol, and filtered (0.22 μm). LC-MS analysis was performed on a UPLC BEH C18 column with gradient elution, using a Q Exactive mass spectrometer in positive/negative electrospray ionization modes. Full scans (m/z 150–2,000) at 35,000 resolution were followed by data-dependent MS/MS with HCD fragmentation[23].

Stability evaluation

BELNs (2.0 mg/mL) were mixed with simulated saliva (pH 6.8, containing 5 mg/mL mucin and 150 mM NaCl) and incubated at 37 °C with stirring (150 rpm). The pH was adjusted to 2.0 with 3 M HCl, followed by the addition of simulated gastric fluid (0.3 mg/mL pepsin). During the 1.5-h gastric digestion, aliquots were periodically collected. Samples were neutralized to pH 5.0 with 0.2 M $NaHCO_3$, mixed with duodenal fluid (10 mg/mL trypsin, 3 mg/mL bile salts), and incubated for 60 min. The pH was then adjusted to 6.5 with 0.1 M $NaHCO_3$ for an additional 1.5 h. After each digestion phase, supernatants were collected by centrifugation at 5,000 × g for 20 min. Particle size and zeta potential were measured at 100, 200, and 300 min using a Nano-ZS90 Nanosizer. For storage stability, these parameters were assessed over 28 d (at 1, 3, 7, 14, and 28 d) under different temperatures (4, −20, and −80 °C).

Liquid chromatography determination of procyanidin B2 levels

Based on previous literature and studies, the detailed experimental steps are as follows[24]: BELNs (3 mL) were mixed with 70% ethanol (1:2, v/v), vortexed (2 min, dark, low temperature), and sonicated on ice (15 min, 150 W, 2 s on/off). After centrifugation (12,000 × g, 20 min, 4 °C), supernatants were collected under N_2. UHPLC-MS/MS analysis was performed on a BEH C18 column with a

16-min gradient (mobile phase A: 2% acetonitrile/0.1% formic acid; B: acetonitrile/0.1% formic acid). ESI ± MS scans covered m/z 70–1,050 at full MS resolution 70,000, and MS/MS resolution 17,500.

Establishment of ALI mouse model

All animal procedures were approved by the Animal Ethics Committee of China Agricultural University (Approval No: AW51214202-5-02). Male C57BL/6J mice (6–8 weeks, 20–23 g, $n = 6$ per group) were obtained from Vital River Laboratory Animal Technology (Beijing) and maintained under specific pathogen-free conditions (12 h light/dark cycle, 22 ± 2 °C)[25]. ALI was induced via intraperitoneal CCl_4 administration (5 mL/kg, 1% v/v in olive oil). Control mice received equivalent volumes of saline through the same administration route. The experimental groups were designated as follows: wild-type control (CK), CCl_4 model (CCl_4), CCl_4 + low-dose BELNs (BELNs-L, 40 mg/kg/d), and CCl_4 + high-dose BELNs (BELNs-H, 80 mg/kg/d). BELNs were administered by oral gavage for 7 consecutive days, with the final dose administered 24 h prior to CCl_4 injection. Body weight of each mouse was monitored weekly. After the 7-d intervention, mice were fasted for 6 h (8:00 AM to 2:00 PM) before euthanasia. Organ tissues were immediately collected upon sacrifice.

Organ index assessment

The organ index serves as a valuable parameter in toxicological assessment, providing quantitative insights into pathological changes in specific tissues[26]. On the final day, mice were weighed before sacrifice, after which liver and kidney tissues were collected and weighed. The organ index was determined by calculating the ratio of tissue weight (mg) to total body mass (g). Each experimental group contained six independent biological replicates.

Biochemical parameters detection

Blood samples were collected in 1.5 mL sterile centrifuge tubes and allowed to clot at room temperature for 2–4 h. Following centrifugation at 3,000 rpm for 10 min, the supernatant serum was collected. Hepatic biochemical parameters, including ALT and AST, were measured by commercial assay kits (Nanjing Institute of Architectural Bioengineering, China). Each experimental group consisted of six independent biological replicates.

Hematoxylin and Eosin (H&E) staining

Upon sacrifice, liver tissues were harvested and fixed in 4% formaldehyde. After fixation, tissue samples underwent sequential processing including washing, ethanol gradient dehydration, xylene clearing, and paraffin embedding. Sections were cut at 5 μm thickness, dewaxed in xylene, rehydrated through a descending ethanol gradient, and stained with hematoxylin-eosin. Histopathological examination was performed using a CaseViewer digital pathology system.

Immunohistochemistry

Immunohistochemical analysis was performed on formalin-fixed paraffin-embedded murine liver sections according to established protocols[27]. Following deparaffinization and rehydration, antigen retrieval was performed using boiling citrate buffer (5 min, then 20 min microwave at low power). Sections were treated with 3% H_2O_2, washed with PBS, and blocked with 10% sheep serum for 30 min. Primary antibody incubation was conducted overnight at 4 °C, followed by 30-min incubation with biotin-conjugated secondary antibodies. Diaminobenzidine (DAB) was used for color development, and sections were counterstained with hematoxylin. A blinded pathologist evaluated 5 high-magnification fields per slide, counting 100 cells per field for quantitative analysis.

Obervation of mitochondria

Mitochondrial ultrastructure in AML12 cells was examined by TEM. Cell specimens underwent primary fixation using 2.5% glutaraldehyde and 2% paraformaldehyde in 0.1 M cacodylate buffer. Subsequent treatment included post-fixation with 1% osmium tetroxide and staining with 2% uranyl acetate. Specimens underwent ethanol gradient dehydration before embedding in LX112 resin (LADD Research Industries). Ultrathin sections were prepared using a Leica Ultracut UC7 microtome, then stained with uranyl acetate and lead citrate for examination under a JEOL 1400 Plus TEM operating at 120 kV[28].

Distribution of BELNs *in vivo*

DiR-labeled BELNs were administered via oral gavage in 100 μL PBS at a concentration of 2.0 mg/mL. BELN biodistribution was monitored using IVIS Spectrum Imaging Systems (PerkinElmer, USA) at scheduled intervals (0, 2, 6, 12, and 24 h) post-administration.

Cells culture and treatments

Mouse hepatocyte AML12 cells, obtained from the Cell Resource Center of the Institute of Basic Medical Sciences, Chinese Academy of Medical Sciences, were cultured in DMEM/F-12 (1:1) medium containing 10% fetal bovine serum, 1% (v/v) ITS-G (insulin-transferrin-selenium) supplement, and 40 ng/mL dexamethasone. Cells were cultured in a humidified incubator at 37 °C with 5% CO_2.

CCK-8 assay

AML12 cells were plated in 96-well plates and treated with different concentrations of CCl_4 (0, 2, 4, 6, 8, and 10 mM), BELNs (0, 20, 40, 60, 80, 100 μg/mL), and PCB2 (0, 2.5, 5, 10, 20 μM) for 24 h. Cell viability was subsequently assessed using a Cell Counting Kit-8 (C0038, Beyotime Biotechnology, China) following the manufacturer's protocol.

Cellular uptake

AML12 cells were seeded in confocal dishes at a density of 2×10^5 cells per well and cultured overnight. BELNs were subsequently introduced into the culture medium and incubated for 6, 12, and 24-h periods. Following incubation, cells were stained with DiO fluorescent dye and DAPI for 30 min at 37 °C in the dark. Cellular uptake of BELNs was visualized and assessed using live-cell fluorescence microscopy (Carl Zeiss Microscopy GmbH, Germany).

Fe^{2+} determination

Following the manufacturer's protocol, AML12 cells were harvested and intracellular Fe^{2+} levels were detected using a FerroOrange kit (Solarbio, Beijing). Briefly, cells were incubated with the FerroOrange working solution for 30 min under standard culture conditions. Subsequent steps were conducted following the manufacturer's recommended protocols.

ROS measurement

Intracellular ROS levels were quantified by a Reactive Oxygen Species Assay Kit (Beyotime Biotechnology). AML12 cells were

collected, resuspended in diluted DCFH-DA probe solution, and incubated at 37 °C for 20 min. Following three washes with serum-free medium, the cells were either imaged by fluorescence microscopy or analyzed by flow cytometry. All experiments were performed in triplicate.

C11-BODIPY (581/591) assay

Lipid peroxidation was assessed with the BODIPY™ 581/591 C11 fluorescent probe (Thermo Fisher Scientific). This fluorescent indicator exhibits a spectral shift from red fluorescence in the reduced state to green fluorescence upon oxidation, enabling quantitative evaluation of lipid peroxidation levels. Cellular lipid peroxidation was quantified through both confocal microscopy and flow cytometry (BD Biosciences), with subsequent data analysis conducted using FlowJo software.

MDA, SOD, and GSH measurement

Glutathione (GSH) levels in AML12 cells and liver tissues were quantified using a commercial reduced glutathione assay kit (Nanjing Institute of Architectural Bioengineering, China). Following the manufacturer's protocol, samples were processed and reacted with the assay reagents, with absorbance measured at 405 nm. Similarly, malondialdehyde (MDA) content was determined using an MDA assay kit (Beyotime Biotechnology), based on the formation of an MDA-thiobarbituric acid adduct measured at 532 nm. Total superoxide dismutase (SOD) activity was assessed using a WST-8-based assay kit (Beyotime Biotechnology, China), with absorbance readings taken at 450 nm according to the standardized procedures.

Quantitative Real-Time Polymerase Chain Reaction (RT-qPCR)

Total RNA was isolated from hepatic tissues and AML12 cells employing TRIzol reagent (15596018, Ambion, USA), with concentration determination performed on a NanoDrop™ spectrophotometer (Thermo Scientific). cDNA synthesis was performed with a commercial reverse transcription kit (TransGen Biotech, AT311). Quantitative analysis of target gene mRNA expression was performed with the FastKing One-Step RT-PCR Kit (FP205, TIANGEN Biotech, China). The specific primer sequences utilized in this study are provided in Table 1.

Western blot analysis

Protein samples from liver tissues and AML12 cells were quantified using the bicinchoninic acid assay. After electrophoretic separation and polyvinylidene fluoride membrane transfer, membranes were blocked with 5% non-fat milk for 2 h at ambient temperature. Immunoblot analysis included overnight incubation with primary antibodies followed by treatment with horseradish peroxidase-labeled secondary antibodies. Following Tris-Buffered Saline with Tween 20 (TBST) washes, protein bands were visualized using enhanced chemiluminescence reagent. Band intensity was quantified by grayscale analysis with ImageJ software (NIH). The following primary antibodies were employed: GPX4 (Proteintech, 67763-1-Ig), Nrf2 (Abclonal, AP1133), SLC3A2 (Proteintech, 15193-1-AP), SLC7A11 (Proteintech, 32384-1-AP), ACSL4 (Proteintech, 22401-1-AP), ALOX15 (Abcam, ab244205), FTL (Proteintech, 10727-1-AP), FTH1 (Proteintech, 11682-1-AP), p53 (Beyotime, AF7671), TNF-α (Beyotime, AF8208), and SREBP1 (Abcam, ab313881). β-tubulin (Beyotime, AF1216) served as the loading control.

Statistical analysis

All experimental results are expressed as mean ± standard deviation. Statistical analysis was performed using GraphPad Prism 8 software (GraphPad Software, USA), employing one-way ANOVA with Tukey's post-hoc test for multiple group comparisons. Unless otherwise specified, all experiments were performed in triplicate, and data are presented as mean ± standard deviation (SD). Statistical significance was defined as * $p < 0.05$, ** $p < 0.01$, *** $p < 0.001$.

Results

Extraction and characterization of BELNs

BELNs were isolated from fresh blueberries through an optimized ultracentrifugation protocol, as schematically illustrated in Fig. 1a. Specifically, 125 g of fresh blueberries were homogenized and centrifuged sequentially to eliminate plant debris, mucilaginous components, fibrous material, and intact organelles. The purified nanoparticle fraction was subsequently obtained by ultracentrifugation at 150,000 × g for 2 h. Finally, a concentration of 1,735 ± 4.44 μg/mL of BELNs was obtained. Subsequently, the physicochemical properties of BELNs were systematically characterized. Dynamic light scattering analysis revealed that BELNs possessed an average hydrodynamic diameter of approximately 130 nm with a zeta potential of −22.5 mV (Fig. 1b, c). Nanoparticle tracking analysis further confirmed the nanoscale dimensions, showing a mean particle size of 179.2 nm (Fig. 1d). Transmission electron microscopy examination confirmed that BELNs maintain a spherical morphology characterized by a distinct double-layered membrane structure (Fig. 1e). Comprehensive lipidomic profiling demonstrated that the lipid composition of BELNs is predominantly comprised of Triacylglycerol (TG, 31%), Diacylglycerol (DG, 18%), Ceramide (Cer, 13%), and Plasma Free Fatty Acids (PFFA, 13%) (Fig. 1f). Phosphatidylglycerol (PG) and DG, as ubiquitous lipid components in PELNs, facilitate

Table 1. Primer sequences.

Gene	Forward sequences (5'-3')	Reverse sequences (3'-5')
ALOX15	*GGCTCCAACAACGAGGTCTAC*	*AGGTATTCTGACACATCCACCTT*
ACSL4	*CTCACCATTATATTGCTGCCTGT*	*TCTCTTTGCCATAGCGTTTTTCT*
LPCAT3	*GACGGGGACATGGGAGAGA*	*GTAAAACAGAGCCAACGGGTAG*
GPX4	*AGGAGCCAGGAAGTAATCAAGAA*	*GCTAGAGATACCACGCAGGT*
Nrf2	*CTTTAGTCAGCGACAGAAGGAC*	*AGGCATCTTGTTTGGGAATGTG*
Trf	*AGGAGCCAGGAAGTAATCAAGAA*	*GCTAGAGATACCACGCAGGT*
FTH1	*TCCTACGTTTACCTGTCCATGT*	*GTTTGTGCAGTTCCAGTAGTGA*
FTL	*CAGCCTGGTCAATTTGTACCT*	*GCCAATTCGCGGAAGAAGTG*
GAPDH	*GGTTGTCTCCTGCGACTTCA*	*TGGTCCAGGGTTTCTTACTCC*

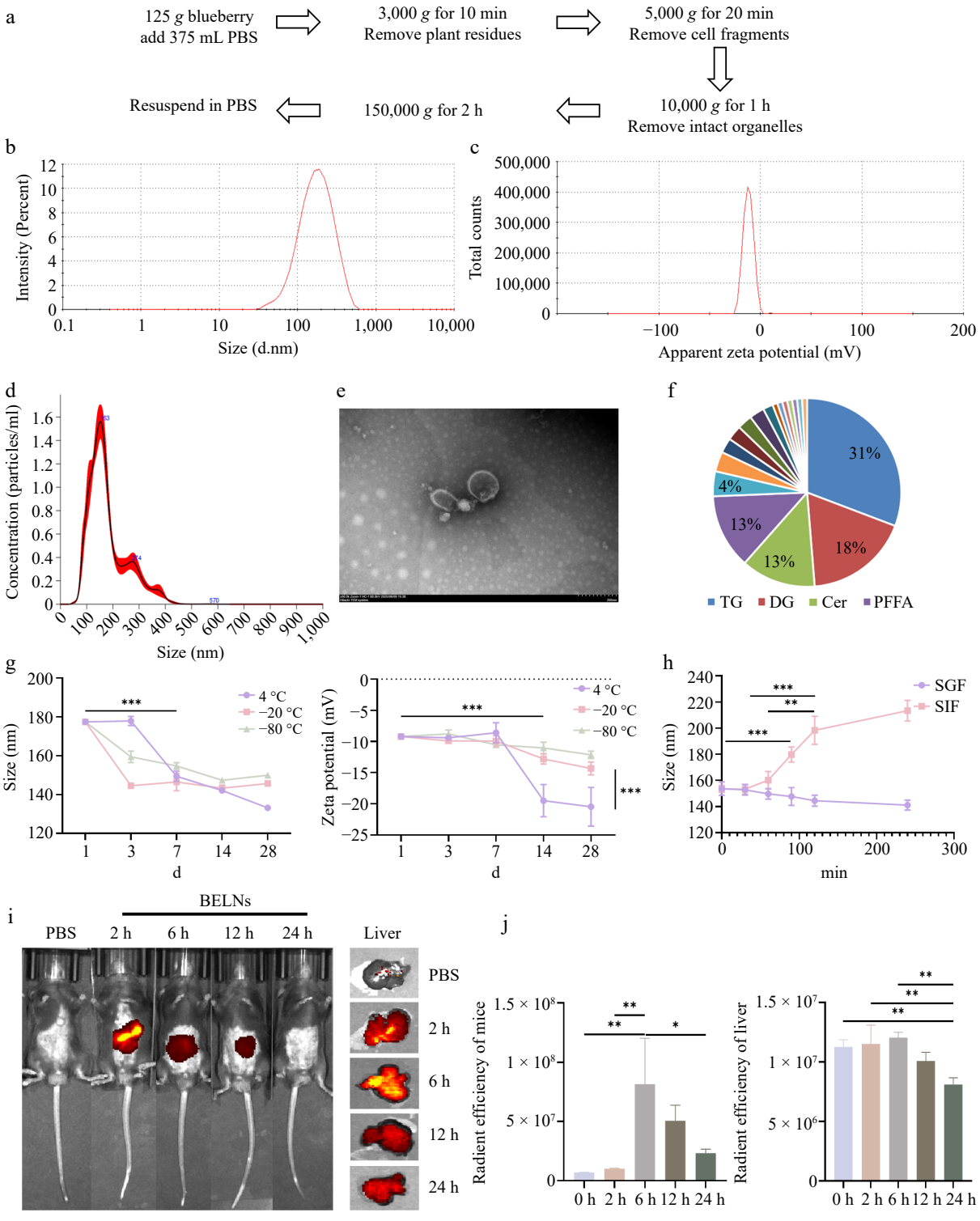

Fig. 1 Isolation and characterization of BELNs. (a) Schematic representation of the BELNs extraction protocol. (b) Size distribution profile measured by DLS. (c) Surface charge characterization through zeta potential analysis. (d) Concentration assessment via nanoparticle tracking analysis. (e) Transmission electron micrographs demonstrating morphological features (scale bar: 200 nm). (f) Comprehensive lipid composition analysis. (g) Stability monitoring under different storage temperatures (4, −20, −80 °C) and duration periods (1, 3, 7, 14, 28 d). (h) Size stability evaluation in simulated gastric and intestinal fluids over a 4-h incubation. (i) Temporal biodistribution patterns following oral administration. (j) Quantitative fluorescence intensity measurements corresponding to the whole-body and liver in Fig. 1i, respectively. * $p < 0.05$, ** $p < 0.01$, *** $p < 0.001$.

membrane fusion, cellular internalization, and signal transduction processes[29]. Cer, generated via sphingomyelin hydrolysis—a crucial precursor for extracellular vesicle (EV) biogenesis—contributes to nanoparticle structure[30].

Stability of BELNs

The stability profile of BELNs was systematically evaluated in order to assess their potential for biomedical applications. The particle size distribution and zeta potential were monitored under

different storage conditions (4, −20, and −80 °C) over time. As demonstrated in Fig. 1g, BELNs demonstrated optimal stability at −80 °C, with minimal variations in both hydrodynamic diameter and surface charge observed over a 1-month period. This confirms the suitability of this storage condition for long-term preservation. The harsh gastrointestinal environment poses significant challenges for orally administered biomaterials. The present study therefore sought to evaluate the digestive stability of BELNs in simulated gastric and intestinal fluids over a 4-h period. As demonstrated in Fig. 1h, the BELNs exhibited notable structural stability in simulated gastric fluid over the duration of the 4-h incubation, thereby evidencing their resilience to gastrointestinal degradation. The mean particle size of BELNs in simulated intestinal fluid demonstrated a consistent increase, reaching stability after 120 min of incubation. Collectively, these findings indicate that BELNs maintain structural integrity and digestive resistance in the gastrointestinal tract, remaining stable in gastric conditions for a minimum of 4 h while undergoing predictable modifications in the intestinal environment.

Fluorescence imaging of BELNs *in vivo*

Oral administration provides significant advantages in clinical oncology, including predictable gastrointestinal absorption, stable blood drug concentrations, and cost-effectiveness through reduced medical resource utilization, while demonstrating superior patient compliance[31]. Based on the above results, the isolated BELNs showed typical exosome-like morphology, suitable particle size for systemic circulation, and good colloidal stability. To further investigate their *in vivo* targeting and biodistribution, we assessed the *in vivo* biodistribution of BELNs following oral administration of fluorescently labeled DiR-BELNs to mice. Control animals received an equivalent volume of PBS. Temporal distribution patterns were monitored at predetermined intervals using non-invasive *in vivo* imaging. As shown in Fig. 1i, j, fluorescence signals became detectable at 2 h post-administration, reached maximum intensity at 6 h, and subsequently declined, with residual signal still observable at 24 h. *Ex vivo* organ imaging confirmed predominant hepatic accumulation, with significantly weaker fluorescence detected in the heart, spleen, lungs, kidneys, and intestines compared to the liver. These findings demonstrate that BELNs undergo efficient metabolic processing *in vivo*, with the liver identified as their primary target organ (Supplementary Fig. S1h).

BELNs protect mice from ALI

To establish an optimal experimental model, a preliminary study was conducted using 7-week-old C57BL/6J mice divided into a control and four CCl_4 treatment groups with varying concentrations. Based on a comprehensive evaluation of serum biochemical parameters and ferroptosis-related gene expression profiles (Supplementary Fig. S1e–S1g), the concentration of 5 mL/kg (1% v/v) was selected for subsequent experimental modeling. To investigate the therapeutic potential of BELNs against ALI, mice were allocated into four experimental groups: control (CK), CCl_4 model, low-dose BELNs (BELNs-L), and high-dose BELNs (BELNs-H), with the treatment protocol outlined in Fig. 2a. Macroscopic examination revealed that CCl_4-induced diffuse steatosis and lipid peroxidation resulted in pronounced pallor and yellowish discoloration of hepatic parenchyma, accompanied by loss of normal dark-red gloss and appearance of diffusely distributed fine granular alterations (Fig. 2b). Body weight remained consistent across all experimental groups during the investigation period (Fig. 2c). Organ coefficient analysis revealed a marked increase in liver index in the CCl_4 model group, which was significantly attenuated by both low and high-dose BELNs treatment. In contrast, renal indices remained comparable across all groups (Fig. 2d). Serum biochemical analysis demonstrated that CCl_4 administration significantly elevated both ALT and AST levels, indicating substantial hepatocellular damage. Both BELN treatment regimens effectively attenuated these elevations, with the high-dose group (BELNs-H) demonstrating superior hepatoprotective efficacy (Fig. 2e). Histopathological examination of liver sections revealed that CCl_4 administration induced characteristic perivascular hepatocyte necrosis surrounding central veins, manifested as eosinophilic staining alterations and disrupted hepatic architecture. Both BELNs-L and BELNs-H treatments markedly attenuated these pathological changes, demonstrating preserved hepatocellular morphology and absence of significant inflammatory infiltration (Fig. 2f).

BELNs alleviate ALI by modulating multiple targets in the ferroptosis pathway

Analysis of ferroptosis-related biomarkers in hepatic tissue demonstrated that CCl_4 challenge significantly increased MDA and Fe^{2+} concentrations while reducing SOD activity and GSH levels (Fig. 3a–d). BELN's treatment effectively counteracted these alterations, with the high-dose regimen showing superior efficacy in mitigating CCl_4-induced iron accumulation, oxidative stress, and lipid peroxidation. Immunohistochemical analysis of 4-hydroxynonenal (4-HNE), a biomarker of lipid peroxidation, demonstrated enhanced positive staining in CCl_4-treated liver tissues compared to controls. BELN administration significantly attenuated this oxidative stress marker, indicating reduced lipid peroxidation (Fig. 3f).

To elucidate the mechanistic basis of BELNs-mediated attenuation of ferroptosis in murine liver, we quantified the expression levels of key regulatory mediators using RT-qPCR and Western blot analyses. The results indicated that CCl_4 challenge significantly upregulates mRNA expression of arachidonate 15-lipoxygenase (ALOX15), acyl-CoA synthetase long-chain family member 4 (ACSL4), and lysophosphatidylcholine acyltransferase 3 (LPCAT3). A contrasting trend was observed between the BELNs-L and BELNs-H groups, wherein the BELNs-H cohort demonstrated more substantial and pronounced alterations relative to the BELNs-L group. Experimental results indicated that CCl_4 administration significantly upregulated the mRNA expression levels of key regulators involved in lipid peroxidation, including ALOX15, ACSL4, and LPCAT3. Both BELNs-L and BELNs-H treatments effectively counteracted this CCl_4-induced upregulation, with the intervention in the BELNs-H group producing a more marked and significant reversal of these expression changes. CCl_4 treatment significantly suppressed the mRNA expression of glutathione peroxidase 4 (GPX4), nuclear factor erythroid 2-related factor 2 (Nrf2), and ferritin heavy chain 1 (FTH1). Both BELNs-L and BELNs-H interventions effectively counteracted this suppression, albeit with distinct efficacies. Specifically, the BELNs-H group elicited a more potent upregulation of GPX4 and Nrf2 mRNA, whereas the BELNs-L group induced a more pronounced increase in FTH1 mRNA expression (Fig. 3e). Western blot analysis corroborated the transcriptional data, demonstrating that BELNs administration upregulated GPX4, Nrf2, and FTH1 protein expression while downregulating ALOX15 and ACSL4 levels. Furthermore, BELNs significantly restored the CCl_4-induced suppression of SLC3A2, SLC7A11, and FTL proteins, while effectively attenuating the CCl_4-mediated upregulation of p53 expression(Fig. 3g, h).

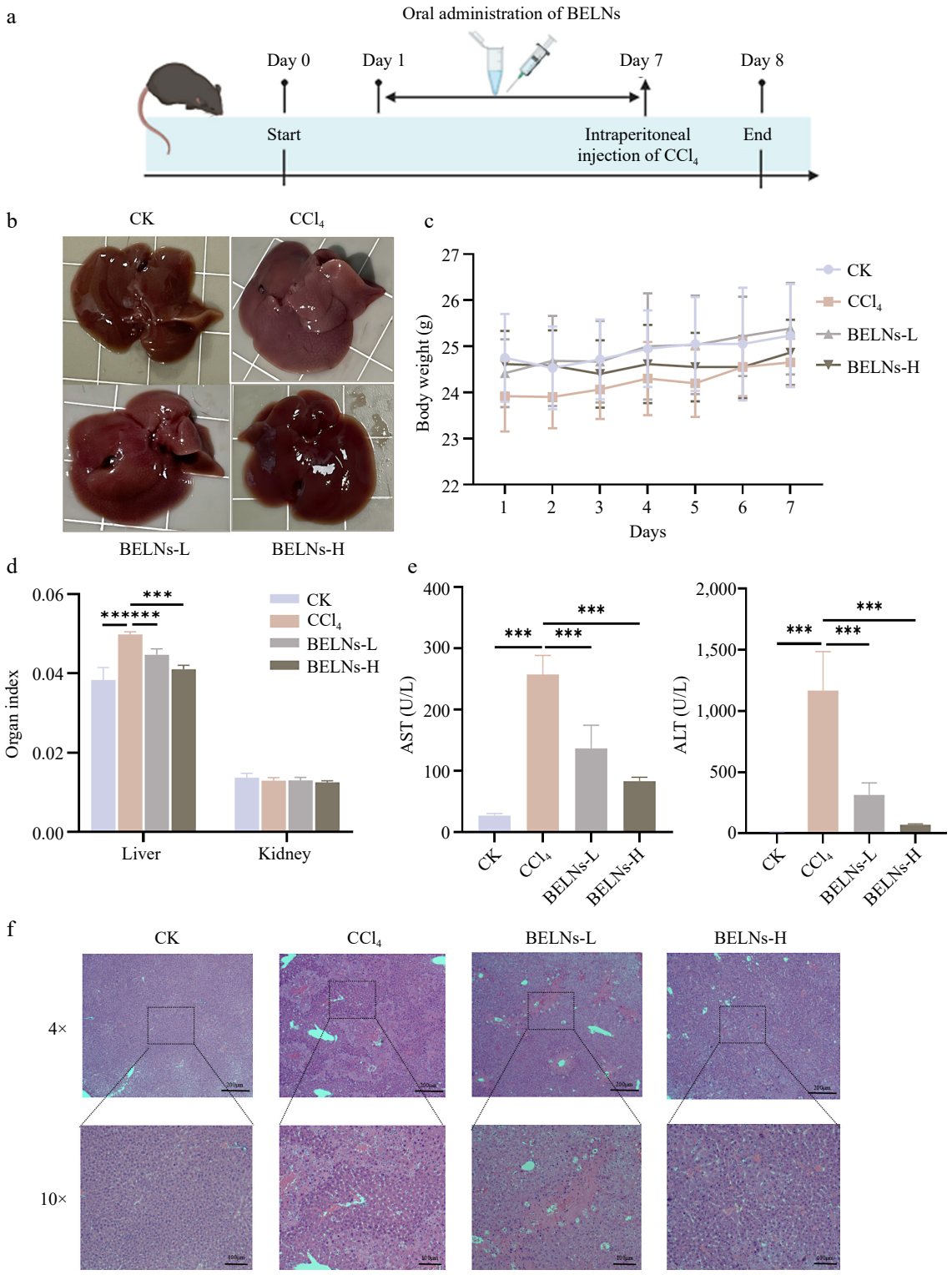

Fig. 2 Protective effects of BELNs against ALI in mice. (a) Schematic diagram of experimental protocol. (b) Representative hepatic morphology and (c) corresponding body weight measurements. (d) Organ index calculations, and (e) serum transaminase profiles. (f) Histopathological examination through H&E staining across treatment conditions. *** $p < 0.001$.

The therapeutic effects of BELNs on ALI *in vitro*

Since the bioactive components of natural nanoparticles primarily execute their therapeutic functions intracellularly, the efficacy of BELNs in treating ALI fundamentally depends on their efficient cellular internalization by hepatocytes. To evaluate cellular internalization efficiency, AML12 cells were treated with DiO-labeled BELNs. As shown in Fig. 4a, BELN internalization exhibited time-dependent characteristics. The intracellular green fluorescence intensity progressively increased over 6, 12, and 24 h of incubation, demonstrating enhanced cellular uptake throughout the 24-h period.

CCK-8 assay results identified 6 mM CCl_4 as the optimal concentration for establishing the AML12 cell injury model. While exposure

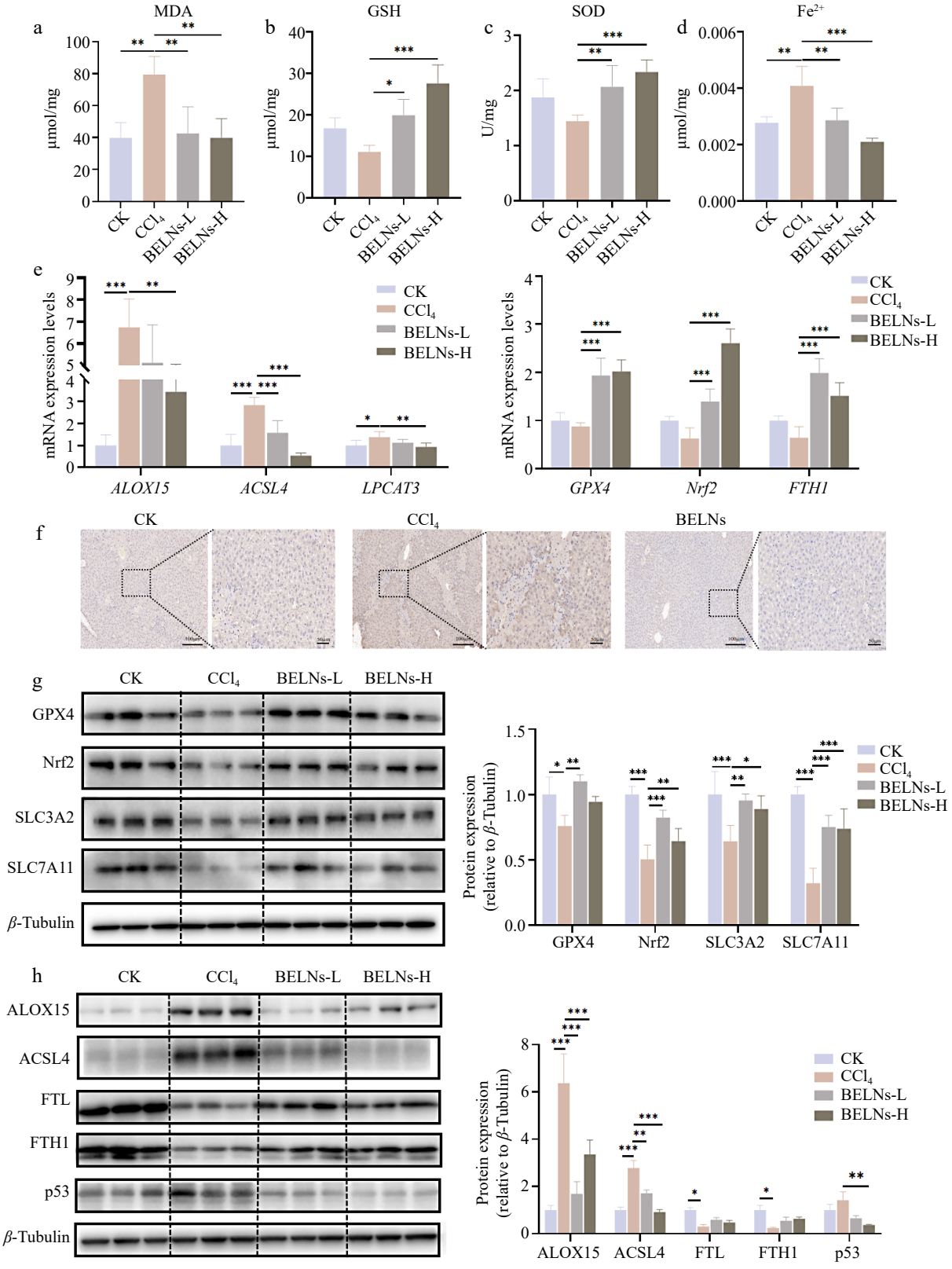

Fig. 3 The expression levels of various indicators in AML12 cells after administration of CCl_4 and BELNs. (a) MDA levels of AML12 cells. (b) GSH levels of AML12 cells. (c) SOD levels of AML12 cells. (d) Fe^{2+} levels of AML12 cells. (e) mRNA expression profiles: left panel shows ALOX15, ACSL4, and LPCAT3; right panel displays GPX4, Nrf2, and FTH1; bottom panel presents IL-6 and TNF-α. (f) Immunohistochemical detection of 4-HNE adducts. (g) Immunoblot analysis of GPX4, Nrf2, SLC3A2, and SLC7A11 proteins. (h) Western blot detection of ALOX15, ACSL4, FTL, FTH1, and p53 expression. β-tubulin were used as loading controls. * $p < 0.05$, ** $p < 0.01$, *** $p < 0.001$.

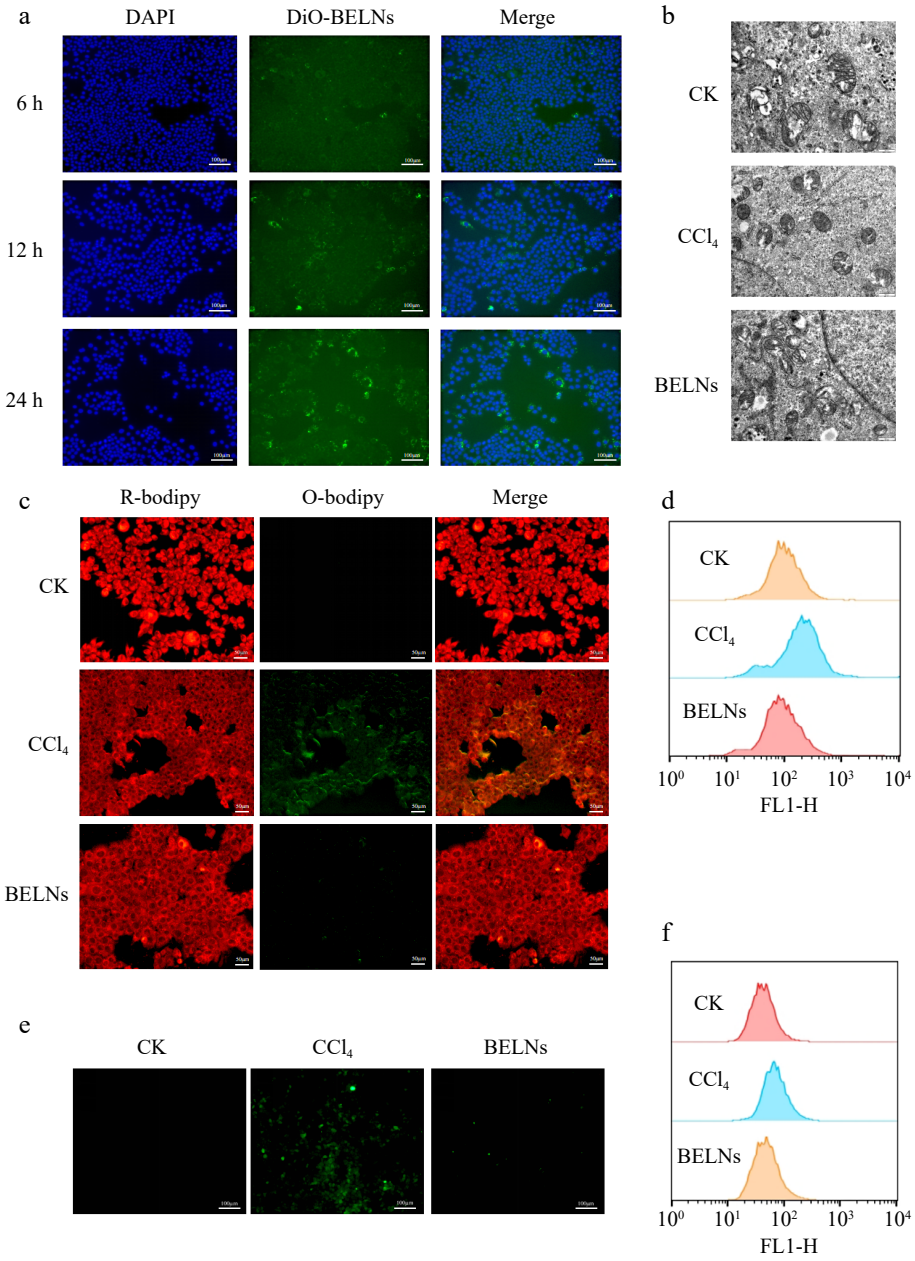

Fig. 4 Cellular uptake and therapeutic effects of BELNs in AML12 hepatocytes. (a) Internalization analysis of BELNs by AML12 cells. (b) Mitochondrial ultrastructure examination via transmission electron microscopy across treatment conditions. (c) BODIPY C11 fluorescence imaging and corresponding flow cytometric quantification (d) of lipid peroxidation. (e) DCFH-DA fluorescence visualization, and (f) subsequent flow cytometric analysis of intracellular ROS levels.

to 8 mM CCl_4 caused a substantial reduction of cell viability to about 60%–70% relative to controls (100%), the 6 mM concentration achieved the desired cytotoxic effect without exceeding the threshold for model establishment (Supplementary Fig. S1b). Utilizing 6 mM CCl_4 as the established model concentration, this investigation evaluated the protective effects of BELNs against oxidative stress and ferroptosis in CCl_4-injured AML12 murine hepatocytes. Treatment with BELNs alone did not induce significant cytotoxicity. Notably, administration of higher BELN concentrations enhanced cell viability, with an increase to 130% observed relative to the control group (Supplementary Fig. S1c). Co-treatment with CCl_4 and varying concentrations of BELNs for 24 h demonstrated a concentration-dependent protective effect. Specifically, high concentrations of BELNs (40 and 80 μg/mL) significantly attenuated CCl_4-induced cytotoxicity, resulting in markedly improved cell viability (Supplementary Fig. S1d).

The progression of ferroptosis and associated lipid peroxidation is characterized by distinct alterations in mitochondrial ultrastructure. These specific morphological changes are recognized as one of the gold standards for the identification of ferroptosis.[32] Transmission electron microscopy analysis of AML12 cells revealed that CCl_4 treatment induced characteristic mitochondrial modifications, featuring diminished organelle size, elevated membrane density, cristae disruption, and outer membrane fragmentation compared to the untreated control group. These morphological changes were substantially ameliorated by BELNs intervention, indicating the potential of BELNs to attenuate ferroptosis (Fig. 4b).

The onset of ferroptosis is featured by concomitant oxidative stress and lipid peroxidation formation. To quantitatively assess these processes, a C11-BODIPY 581/591 fluorescent probe was utilized to monitor lipid peroxidation through the ratiometric measurement of its fluorescence emission shift. Simultaneously, intracellular ROS levels were quantified using the DCFH-DA fluorescent probe, which undergoes oxidation to generate quantifiable fluorescence within the cellular environment. To further verify the occurrence of ferroptosis, AML12 cells in the model group were treated with 6 mM CCl_4, while the intervention group received supplementary administration of 100 μg/mL BELNs. As illustrated in Fig. 4c, comparative analysis revealed a substantial intensification of green fluorescence in the CCl_4 group relative to the control, whereas the BELNs intervention group exhibited a marked attenuation of this fluorescent signal. These observations indicate that BELN treatment effectively attenuates CCl_4-induced lipid peroxidation in AML12 cells. No significant intergroup differences were detected in red fluorescence intensity. Flow cytometric analysis confirmed that BELNs administration significantly attenuated CCl_4-induced lipid peroxidation in AML12 cells, demonstrating a consistent trend with prior morphological observations (Fig. 4d). Furthermore, BELNs treatment effectively suppressed the CCl_4-triggered accumulation of intracellular ROS. This protective effect against oxidative stress was similarly verified through flow cytometry, showing concordant results (Fig. 4e, f).

In order to provide further validation of the effects of BELNs on CCl_4-induced oxidative stress and ferroptosis in AML12 cells, changes in MDA, GSH, and SOD levels were quantified. The model group demonstrated elevated MDA levels in conjunction with diminished SOD and GSH levels. The administration of BELN therapy resulted in the reversal of these alterations (Fig. 5a–c). The detection of Fe^{2+} resulted in the identification of considerably elevated Fe^{2+} concentrations in the CCl_4 group in comparison with the control group. Conversely, the BELNs group demonstrated a conspicuously diminished level of Fe^{2+}. This finding suggests that BELNs reduced Fe^{2+} levels in AML12 cells (Fig. 5d).

BELNs treat ALI via the ACSL4/LPCAT3/ALOX15 signaling pathway

To investigate the molecular mechanisms underlying BELNs' modulation of ferroptosis in AML12 cells, we performed RT-qPCR and Western blot analyses on key ferroptosis-associated genes. The results demonstrated that CCl_4 treatment significantly upregulated mRNA expression of ALOX15, ACSL4, and LPCAT3—all established mediators of ferroptosis. Notably, BELN administration effectively reversed these CCl_4-induced expression alterations (Fig. 5e). Furthermore, BELN treatment effectively restored the mRNA expression of GPX4, Nrf2, FTH1, and Ferritin Light Chain (FTL) that had been suppressed by CCl_4, while concurrently suppressing the CCl_4-induced upregulation of Transferrin (Trf) mRNA. Western blot analysis confirmed protein-level consistency with these RT-qPCR findings (Fig. 5f). Subsequent verification using the ferroptosis inhibitor Fer-1 as a positive control further supported these results. Collectively, these data demonstrate that BELNs suppress the CCl_4-activated ACSL4/LPCAT3/ALOX15 signaling axis in AML12 cells (Fig. 5g).

PCB2 is one of the primary active ingredients in BELNs

Previous analytical studies have confirmed that PELNs are enriched with a diverse array of bioactive constituents, including complex lipid species, functional proteins, and nucleic acids[33]. To identify the principal bioactive component in BELNs responsible for mitigating ALI, we conducted further *in vitro* validation using AML12 cells. Liquid chromatography analysis revealed a substantial presence of PCB2 in BELNs, quantified at 6 μM (Fig. 6a). Molecular docking analysis employing CB-Dock software predicted the binding conformation between ALOX15 and PCB2, with Fig. 6b presenting the theoretically modeled complex structure in the absence of experimental crystallographic data. Cytotoxicity assessment revealed that PCB2 was well-tolerated, with no significant cytotoxicity observed at concentrations up to 20 μM (Supplementary Fig. S1a). Biochemical analysis of ferroptosis-related markers in AML12 cells demonstrated that CCl_4 exposure significantly elevated MDA and Fe^{2+} concentrations while reducing SOD and GSH activities. These pathological alterations were effectively reversed by PCB2 treatment, as illustrated in Fig. 6c–f.

To further substantiate the protective effects of PCB2 against CCl_4-induced cellular damage, we evaluated oxidative stress and lipid peroxidation through fluorescent probes. As demonstrated in Fig. 6h, comparative analysis revealed a significant intensification of green fluorescence in the CCl_4 group compared to controls, whereas PCB2 treatment markedly attenuated this fluorescent signal, indicating its efficacy in reducing both ROS generation and lipid peroxidation. No significant variations in red fluorescence intensity were observed across experimental groups. Concurrently, PCB2 intervention effectively suppressed the CCl_4-induced accumulation of ROS in AML12 cells. Flow cytometric analyses consistently confirmed that PCB2 significantly attenuated both lipid peroxidation and ROS elevation, demonstrating concordant trends with prior fluorescence microscopy observations (Fig. 6i–k).

To determine whether PCB2's mechanism of action corresponds to that of BELNs in ameliorating acute cellular injury, we performed RT-qPCR and Western blot analyses on ferroptosis-related markers. The results demonstrated that PCB2 treatment effectively counteracted the CCl_4-induced upregulation of ALOX15, ACSL4, LPCAT3, and Trf mRNA expression. Concurrently, PCB2 restored the suppressed expression of GPX4, Nrf2, and FTH1 mRNA. Western blot analysis confirmed full consistency with these transcriptional profiles (Fig. 6l, m), indicating PCB2 mediates its protective effects through the same molecular pathways as BELNs.

Discussion

BELNs isolation, characterization, and biosafety

In this investigation, nanoparticles were isolated from fresh blueberry fruit via ultracentrifugation. Characterization via TEM, DLS, and zeta potential confirmed that BELNs possess nanoscale vesicular structures. Lipidomic and metabolomic analyses revealed diverse bioactive compounds. Biosafety assessment revealed excellent biocompatibility, with no cytotoxicity toward AML12 cells and even promotion of cellular proliferation. *In vivo* evaluations further indicated favorable tissue targeting capabilities. Furthermore, PCB2 was identified as the principal bioactive constituent within BELNs. These nanoparticles demonstrate high yield, extraction stability, and exceptional biocompatibility, highlighting their substantial potential as natural nanotherapeutic agents and drug delivery vehicles.

BELNs as nanocarriers for liver disease therapy

As a multi-kinase inhibitor targeting oncogenic signaling pathways, sorafenib became the inaugural systemic treatment approved

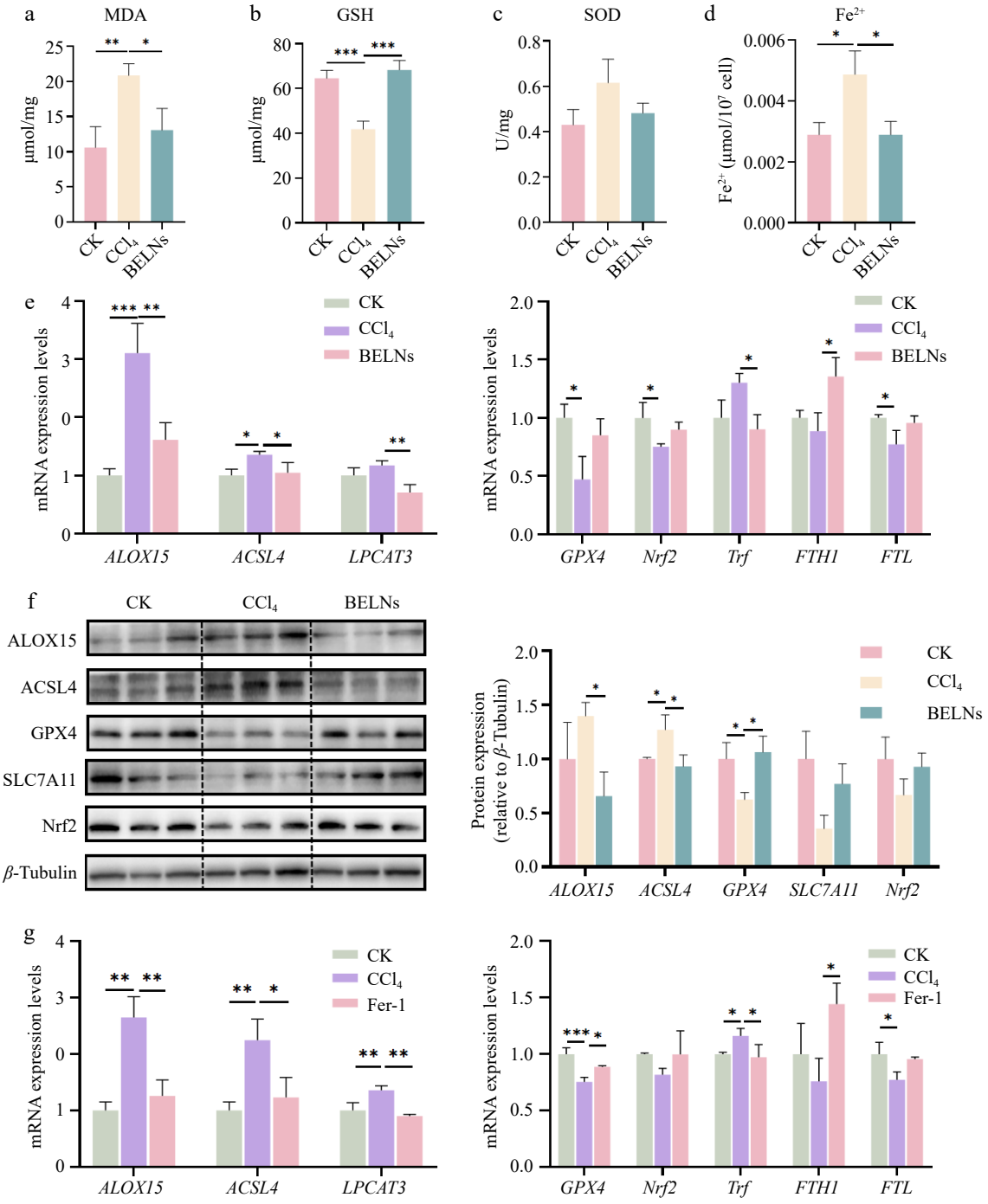

Fig. 5 The expression levels of various indicators in AML12 cells after administration of CCl_4, BELNs and Fer-1. (a) MDA levels of AML12 cells. (b) GSH levels of AML12 cells. (c) SOD levels of AML12 cells. (d) Fe^{2+} levels of AML12 cells. (e) mRNA expression analysis: left - ALOX15, ACSL4, LPCAT3; right - GPX4, Nrf2, Trf, FTH1, FTL. (f) Protein immunoblots of key pathway components (ALOX15, ACSL4, GPX4, SLC7A11, Nrf2). β-tubulin was used as loading controls. (g) qPCR results for GPX4, Nrf2, Trf, FTH1, and FTL expression following Fer-1 treatment. * $p < 0.05$, ** $p < 0.01$, *** $p < 0.001$.

by the US Food and Drug Administration (FDA), demonstrating overall survival benefits in patients with advanced hepatocellular carcinoma. Research has verified sorafenib's therapeutic efficacy in CCl_4-induced ALI models[34]. While clinical evidence confirms its survival benefits as initial therapy for innovative hepatocellular carcinoma, acquired resistance frequently develops. This typically occurs within 6 months of therapy initiation. Our findings position BELNs as promising therapeutic candidates for hepatic pathologies. Previous investigations have established the exceptional drug-loading capacity of PELNs, supporting their pharmaceutical applicability[35]. Subsequent investigations should therefore evaluate BELNs as nanocarriers for delivering sorafenib and silymarin in ALI treatment. Given the established delivery efficiency of PELNs, comparative studies between BELN-encapsulated PCB2 and free PCB2 formulations would be particularly warranted. The phospholipid bilayer architecture of BELNs may stabilize PCB2 against enzymatic degradation and pH fluctuations, thereby enhancing its biodistribution and targeted delivery to distant organs.

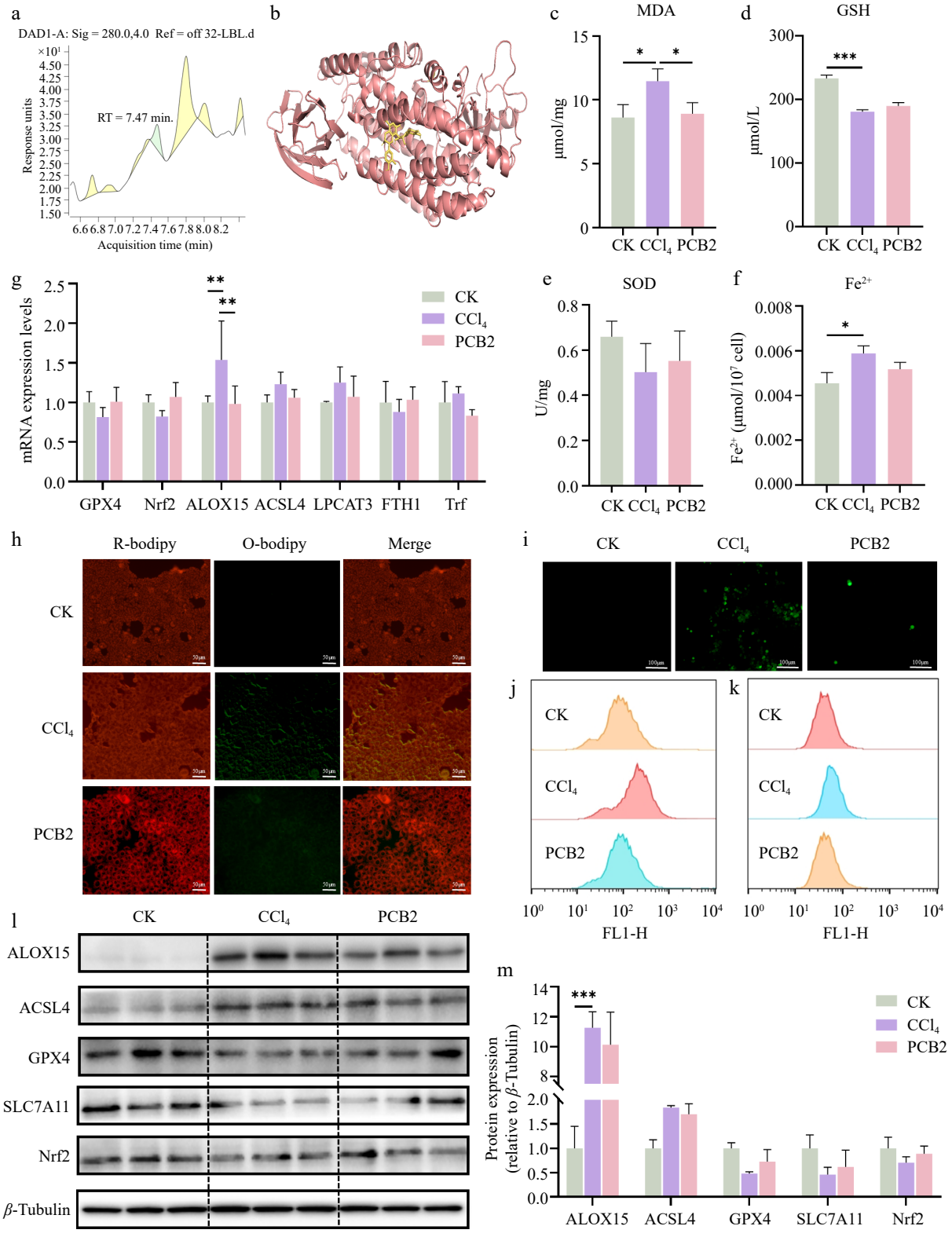

Fig. 6 The expression levels of different indicators in AML12 cells treated with CCl_4 and PCB2. (a) Non-targeted metabolomics of BELNs. (b) Molecular docking analysis using CB-Dock predicted specific binding interactions between ALOX15 and PCB2, revealing potential active sites and binding affinities. (c) MDA levels of AML12 cells. (d) GSH levels of AML12 cells. (e) SOD levels of AML12 cells. (f) Fe^{2+} levels of AML12 cells. (g) qPCR results for GPX4, Nrf2, ALOX15, ACSL4, LPCAT3, FTH1, and Trf expression. (h)–(k) Lipid peroxidation (C11) and ROS detection by fluorescence microscopy and flow cytometry. (l)–(m) Protein expression analysis of key pathway regulators. β-tubulin was used as loading controls. * $p < 0.05$, ** $p < 0.01$, *** $p < 0.001$.

Comparison with other food-derived exosome-like nanoparticles (FDELNs)

FDELNs exhibit excellent targeted delivery capabilities. As early as 2016, research on milk-derived exosomes for drug delivery was already underway[36]. In addition, many PELNs have demonstrated promising effects in improving liver diseases. Beyond plants, other FDELNs exhibit similar benefits. For instance, exosomes from composite milk possess anti-liver fibrosis properties[37], honey-derived nanoparticles protect elderly individuals from non-alcoholic steatohepatitis[38], and probiotic-derived exosomes alleviate alcoholic liver disease by suppressing intestinal miR-194[39].

PCB2: the key bioactive component and its applications

This study elucidates the therapeutic mechanism of BELNs. Specifically, the encapsulated effector components were identified as direct mediators that regulate ferroptosis and lipid peroxidation. PCB2 is a naturally occurring polyphenolic compound commonly extracted from fruits, seeds, and leaves of botanicals including *Vitis vinifera*, *Crataegus pinnatifida*, *Glycine max*, and *Vaccinium* species. PCB2 demonstrates multifaceted biological activities. It exhibits therapeutic potential for multiple pathological conditions, including diabetic complications, diabetes mellitus, non-alcoholic fatty liver disease, and atherosclerosis. Its mechanistic basis has been partially characterized, involving modulation of MAPK, NF-κB, PI3K/Akt, apoptotic signaling, and Nrf-2/HO-1 pathways[40]. However, its mechanisms related to ferroptosis remain largely unexplored, highlighting the significance of our investigation for advancing PCB2's therapeutic development. Previous studies have established PCB2's protective efficacy against CCl_4-induced ALI[41], diet-induced obesity and NAFLD via gut microbiota modulation[42], and FFA-induced hepatic lipid accumulation via TFEB-dependent lysosomal regulation[43]. These established mechanisms provide a theoretical foundation for our investigation into PCB2's role in regulating hepatocyte lipid peroxidation.

BELNs inhibit ferroptosis via the lipid peroxidation pathway

Research confirms that CCl_4-induced oxidative stress significantly increased ROS and MDA levels, while concurrently decreasing GSH and SOD in AML12 cells. BELNs treatment counteracted these effects by diminishing ROS and MDA accumulation, enhancing SOD activity, and increasing the GSH/GSSG ratio, ultimately relieving oxidative injury in murine hepatocytes. ROS are pivotal in triggering ferroptosis by actively participating in the generation of lipid peroxides[44]. As a terminal product of lipid peroxidation, MDA functions as a recognized biomarker for evaluating oxidative stress and ferroptosis progression, directly reflecting the extent of membrane lipid damage[45]. SOD provides cellular defense by catalyzing the transformation of superoxide radicals into hydrogen peroxide and molecular oxygen, thereby mitigating oxidative stress[46]. During ferroptosis, the antioxidant defense system becomes overwhelmed. This system, which includes enzymes such as SOD, subsequently fails to neutralize excessive ROS. This insufficiency leads to uncontrolled lipid peroxidation[47,48]. SLC7A11 functions as the light chain subunit, while SLC3A2 serves as the heavy chain subunit of the system xc^- transporter. This heterodimeric complex mediates the 1:1 antiport of extracellular cysteine and intracellular glutamate, thereby providing the cysteine substrate required for GSH biosynthesis[49]. The synthesized GSH subsequently acts as an important cofactor for GPX4 during the catalytic reduction of lipid peroxides[50]. GPX4 catalyzes the conversion of lipid hydroperoxides to their corresponding alcohol derivatives, thereby inhibiting lipid peroxidation propagation and serving as a master regulator of the ferroptotic pathway[51]. Nrf2 confers hepatoprotection against oxidative damage through its interaction with antioxidant response elements (ARE)[52]. Additionally, Nrf2 modulates hepatic iron homeostasis by regulating ferritin synthesis and degradation pathways, consequently influencing cellular susceptibility to ferroptosis. Our findings demonstrate that BELN treatment significantly reduced MDA accumulation while enhancing GSH and SOD levels. Furthermore, BELNs upregulated both transcriptional and translational SLC7A11 and GPX4 expression compared to the CCl_4 group. Collectively, these results indicate that BELNs effectively attenuated ferroptosis in hepatocytes.

BELNs suppress the ACSL4–ALOX15 axis to inhibit ferroptosis

Ferroptosis represents a distinct iron-dependent regulated cell death modality. It is characterized by unique biochemical and morphological features that differentiate it from classical apoptosis, necrotic death, and autophagic processes, and is primarily initiated by the pathological accumulation of ROS and lipid peroxides[53]. ACSL4, a crucial isoenzyme in polyunsaturated fatty acid metabolism, localizes to mitochondria, peroxisomes, and endoplasmic reticulum. It modulates cellular susceptibility to ferroptosis through its regulatory role in determining lipid composition[54]. As a key promoter of ferroptosis, ACSL4 inhibition represents a crucial regulatory mechanism for its suppression. ACSL4 activates polyunsaturated fatty acids and, in coordination with LPCAT3, facilitates their incorporation into phosphatidylcholines to form Polyunsaturated Fatty Acids-Phospholipids (PUFA-PLs). PLs readily undergo ALOX15-mediated enzymatic peroxidation, driving the execution of ferroptosis[55]. The ACSL4/ALOX15 axis constitutes one of the principal regulatory systems driving ferroptosis progression[56]. Based on this finding, we further considered why BELNs and PCB2 specifically target the ACSL4/ALOX15 axis. Notably, SIRT5 has been identified as an upstream regulator of the ACSL4/LPCAT3/ALOX15 axis in HCC. In this context, Arachidonic Acid (AA) upregulates this axis via SIRT5, thereby inducing ferroptosis[57]. Moreover, multiple studies have demonstrated that the sirtuin family is closely associated with both the therapeutic effects and carrier properties of exosomes[58,59]. Furthermore, the progression of lipid peroxidation and ferroptosis is featured by the downregulation of FTH1 and FTL expression[60]. Concurrently, nuclear receptor coactivator 4 (NCOA4) mediates selective ferritinophagy by targeting FTH1, thereby influencing ferroptosis through iron homeostasis modulation[61,62]. Our experimental data corroborate these mechanistic relationships.

Limitations and future directions

We acknowledge several limitations in the present study. First, blueberry juice should be included as an additional control in future experiments. This will allow a comparison between the effects of BELNs and blueberry juice alone. The goal is to evaluate potential advantages of BELNs over the whole juice matrix, such as improved stability, bioavailability, delivery efficiency, or bioactivity. These findings will lay a theoretical foundation for future industrial and clinical applications. Second, the specific molecular interaction between PCB2 and the ALOX15/ACSL4 complex requires experimental validation beyond *in silico* docking predictions. Third, we can further

investigate how blueberry variety, origin, and processing methods affect BELNs' yield and activity. Stability experiments under simulated food processing or storage conditions can also be performed. Additionally, the compatibility of BELNs with different food matrices, such as beverages and solid foods, can be examined. These efforts will strengthen the practical relevance of this study.

Conclusions

In conclusion, this study demonstrates that BELNs protect against ALI by targeting the ACSL4–ALOX15-ferroptosis axis. BELNs are natural, orally administered nanoparticles. PCB2, as the key active constituent, recapitulates this protective effect by suppressing ferroptosis and lipid peroxidation. These findings reveal a previously unrecognized mechanism by which FDELNs modulate a specific ferroptosis pathway. This highlights their potential as a promising therapeutic strategy for ALI with promising translational prospects. As functional food ingredients, these findings position BELNs as promising candidates for incorporation into health-promoting food products or nutraceutical formulations.

Ethical statements

All animal experiments were approved by the Ethics Committee of the Center for Animal Experiments of China Agricultural University (Approval number: AW51214202-5-02).

Author contributions

The authors confirm their contributions to the paper as follows: conceived the experiments and supervised the study: Huang K, He X; performed the experiments, analyzed the data, and prepared, wrote and revised the manuscript: Liu R, Zhang F; provided insightful suggestions: Zhang C, Xu T, Wang T, Wang Y, Ding Y. All authors reviewed the results and approved the final version of the manuscript.

Data availability

All data generated or analyzed during this study are included in this published article and its supplementary information files. The original data generated during this research are available from the corresponding author on reasonable request.

Acknowledgments

We would like to thank the Artemether and the NAFLD Target Proteins Project of China Agricultural University.

Conflict of interest

The authors declare that they have no known competing financial interests or personal relationships that could have appeared to influence the work reported in this paper.

Supplementary information accompanies this paper online at: https://doi.org/10.48130/fia-0026-0023.

Dates

Received 28 January 2026; Revised 3 April 2026; Accepted 21 April 2026; Published online 25 June 2026

References

[1] Mustafa AM, Angeloni S, Abouelenein D, Acquaticci L, Xiao J, et al. 2022. A new HPLC-MS/MS method for the simultaneous determination of 36 polyphenols in blueberry, strawberry and their commercial products and determination of antioxidant activity. *Food Chemistry* 367:130743

[2] Duan Y, Tarafdar A, Chaurasia D, Singh A, Bhargava PC, et al. 2022. Blueberry fruit valorization and valuable constituents: a review. *International Journal of Food Microbiology* 381:109890

[3] Herrera-Balandrano DD, Chai Z, Hutabarat RP, Beta T, Feng J, et al. 2021. Hypoglycemic and hypolipidemic effects of blueberry anthocyanins by AMPK activation: *in vitro* and *in vivo* studies. *Redox Biology* 46:102100

[4] Yan Y, Zhang F, Chai Z, Liu M, Battino M, et al. 2019. Mixed fermentation of blueberry pomace with *L. rhamnosus GG* and *L. plantarum-1*: enhance the active ingredient, antioxidant activity and health-promoting benefits. *Food and Chemical Toxicology* 131:110541

[5] Negi T, Kumar Y, Sirohi R, Singh S, Tarafdar A, et al. 2022. Advances in bioconversion of spent tea leaves to value-added products. *Bioresource Technology* 346:126409

[6] Kuntz S, Kunz C, Rudloff S. 2017. Inhibition of pancreatic cancer cell migration by plasma anthocyanins isolated from healthy volunteers receiving an anthocyanin-rich berry juice. *European Journal of Nutrition* 56:203–214

[7] Whyte AR, Rahman S, Bell L, Edirisinghe I, Krikorian R, et al. 2021. Improved metabolic function and cognitive performance in middle-aged adults following a single dose of wild blueberry. *European Journal of Nutrition* 60:1521–1536

[8] Zhuge Q, Zhang Y, Liu B, Wu M. 2020. Blueberry polyphenols play a preventive effect on alcoholic fatty liver disease C57BL/6 J mice by promoting autophagy to accelerate lipolysis to eliminate excessive TG accumulation in hepatocytes. *Annals of Palliative Medicine* 9:1045–1054

[9] Wang Y, Cheng M, Zhang B, Nie F, Jiang H. 2013. Dietary supplementation of blueberry juice enhances hepatic expression of metallothionein and attenuates liver fibrosis in rats. *PLoS One* 8:e58659

[10] Feng J, Wang C, Liu T, Li J, Wu L, et al. 2019. Procyanidin B2 inhibits the activation of hepatic stellate cells and angiogenesis via the Hedgehog pathway during liver fibrosis. *Journal of Cellular and Molecular Medicine* 23:6479–6493

[11] Ju S, Mu J, Dokland T, Zhuang X, Wang Q, et al. 2013. Grape exosome-like nanoparticles induce intestinal stem cells and protect mice from DSS-induced colitis. *Molecular therapy : the journal of the American Society of Gene Therapy* 21:1345–1357

[12] Wang Q, Ren Y, Mu J, Egilmez NK, Zhuang X, et al. 2015. Grapefruit-derived nanovectors use an activated leukocyte trafficking pathway to deliver therapeutic agents to inflammatory tumor sites. *Cancer Research* 75:2520–2529

[13] Zhang M, Viennois E, Prasad M, Zhang Y, Wang L, et al. 2016. Edible ginger-derived nanoparticles: a novel therapeutic approach for the prevention and treatment of inflammatory bowel disease and colitis-associated cancer. *Biomaterials* 101:321–340

[14] Takakura H, Nakao T, Narita T, Horinaka M, Nakao-Ise Y, et al. 2022. *Citrus limon L.*-derived nanovesicles show an inhibitory effect on cell growth in p53-inactivated colorectal cancer cells via the macropinocytosis pathway. *Biomedicines* 10:1352

[15] Liu R, Zhang F, He X, Huang K. 2025. Plant derived exosome-like nanoparticles and their therapeutic applications in glucolipid metabolism diseases. *Journal of Agricultural and Food Chemistry* 73:6385–6399

[16] Thawley V. 2017. Acute liver injury and failure. *Veterinary Clinics of North America: Small Animal Practice* 47:617–630

[17] Ramachandran A, Jaeschke H. 2018. Oxidative stress and acute hepatic injury. *Current Opinion in Toxicology* 7:17–21

[18] Maiwall R, Kulkarni AV, Arab JP, Piano S. 2024. Acute liver failure. *The Lancet* 404:789–802

[19] Lu K, Shen SY, Luo OY, Lu Y, Shi TS, et al. 2022. Manipulating PP2Acα-ASK-JNK signaling to favor apoptotic over necroptotic hepatocyte fate reduces the extent of necrosis and fibrosis upon acute liver injury. *Cell Death & Disease* 13:985

[20] Lin F, Chen W, Zhou J, Zhu J, Yao Q, et al. 2022. Mesenchymal stem cells protect against ferroptosis via exosome-mediated stabilization of SLC7A11 in acute liver injury. *Cell Death & Disease* 13:271

[21] De Robertis M, Sarra A, D'Oria V, Mura F, Bordi F, et al. 2020. Blueberry-derived exosome-like nanoparticles counter the response to TNF-α-induced change on gene expression in EA.hy926 cells. *Biomolecules* 10:742

[22] Rezakhani L, Alizadeh M, Sharifi E, Soleimannejad M, Alizadeh A. 2021. Isolation and characterization of crab haemolymph exosomes and its effects on breast cancer cells (4T1). *Cell Journal* 23:658–664

[23] Wang F, Li L, Deng J, Ai J, Mo S, et al. 2025. Lipidomic analysis of plant-derived extracellular vesicles for guidance of potential anti-cancer therapy. *Bioactive Materials* 46:82–96

[24] Tian Y, Liu X, Chen X, Wang B, Dong M, et al. 2024. Integrated untargeted metabolome, full-length sequencing and transcriptome analyses reveal the mechanism of flavonoid biosynthesis in blueberry (*Vaccinium* spp.) fruit. *International Journal of Molecular Sciences* 25:4137

[25] Wang Y, Zhang Q, Kan M, Chang F, He X, et al. 2024. Multi-omics analysis of Au@Pt nanozyme for the modulation of glucose and lipid metabolism. *Journal of Nanobiotechnology* 22:524

[26] Sellers RS, Mortan D, Michael B, Roome N, Johnson JK, et al. 2007. Society of toxicologic pathology position paper: organ weight recommendations for toxicology studies. *Toxicologic Pathology* 35:751–755

[27] Yi M, Zhang D, Song B, Zhao B, Niu M, et al. 2022. Increased expression of ECT2 predicts the poor prognosis of breast cancer patients. *Experimental Hematology & Oncology* 11:107

[28] Liang FG, Zandkarimi F, Lee J, Axelrod JL, Pekson R, et al. 2024. OPA1 promotes ferroptosis by augmenting mitochondrial ROS and suppressing an integrated stress response. *Molecular Cell* 84:3098–3114.e6

[29] Liu H, Dong T, Dong C, Yang F, Zhou Q, et al. 2025. Plant-derived exosome-like nanovesicles: a novel therapeutic perspective for skin diseases. *Journal of Nanobiotechnology* 23:640

[30] Trajkovic K, Hsu C, Chiantia S, Rajendran L, Wenzel D, et al. 2008. Ceramide triggers budding of exosome vesicles into multivesicular endosomes. *Science* 319:1244–1247

[31] Yang M, Guo J, Li J, Wang S, Sun Y, et al. 2025. Platycodon grandiflorum-derived extracellular vesicles suppress triple-negative breast cancer growth by reversing the immunosuppressive tumor microenvironment and modulating the gut microbiota. *Journal of Nanobiotechnology* 23:92

[32] Tadokoro T, Ikeda M, Ide T, Deguchi H, Ikeda S, et al. 2020. Mitochondria-dependent ferroptosis plays a pivotal role in doxorubicin cardiotoxicity. *JCI Insight* 5:e132747

[33] Lian MQ, Chng WH, Liang J, Yeo HQ, Lee CK, et al. 2022. Plant-derived extracellular vesicles: recent advancements and current challenges on their use for biomedical applications. *Journal of Extracellular Vesicles* 11:e12283

[34] Yuan S, Wei C, Liu G, Zhang L, Li J, et al. 2022. Sorafenib attenuates liver fibrosis by triggering hepatic stellate cell ferroptosis via HIF-1α/SLC7A11 pathway. *Cell Proliferation* 55:e13158

[35] You JY, Kang SJ, Rhee WJ. 2021. Isolation of cabbage exosome-like nanovesicles and investigation of their biological activities in human cells. *Bioactive Materials* 6:4321–4332

[36] Munagala R, Aqil F, Jeyabalan J, Gupta RC. 2016. Bovine milk-derived exosomes for drug delivery. *Cancer Letters* 371:48–61

[37] Gong L, Zhou H, Zhang Y, Wang C, Fu K, et al. 2023. Preparation of Phillygenin-Hyaluronic acid composite milk-derived exosomes and its anti-hepatic fibrosis effect. *Materials Today Bio* 23:100804

[38] Liu B, Nguyen PL, Yu H, Li X, Wang H, et al. 2024. Honey vesicle-like nanoparticles protect aged liver from non-alcoholic steatohepatitis. *Acta Pharmaceutica Sinica B* 14:3661–3679

[39] Jiang M, Li F, Liu Y, Gu Z, Zhang L, et al. 2023. Probiotic-derived nanoparticles inhibit ALD through intestinal miR194 suppression and subsequent FXR activation. *Hepatology* 77:1164–1180

[40] Chen J, Zhong K, Jing Y, Liu S, Qin S, et al. 2023. Procyanidin B2: a promising multi-functional food-derived pigment for human diseases. *Food Chemistry* 420:136101

[41] Yang BY, Zhang XY, Guan SW, Hua ZC. 2015. Protective effect of procyanidin B2 against CCl_4-induced acute liver injury in mice. *Molecules* 20:12250–12265

[42] Xing YW, Lei GT, Wu QH, Jiang Y, Huang MX. 2019. Procyanidin B2 protects against diet-induced obesity and non-alcoholic fatty liver disease via the modulation of the gut microbiota in rabbits. *World Journal of Gastroenterology* 25:955–966

[43] Su H, Li Y, Hu D, Xie L, Ke H, et al. 2018. Procyanidin B2 ameliorates free fatty acids-induced hepatic steatosis through regulating TFEB-mediated lysosomal pathway and redox state. *Free Radical Biology and Medicine* 126:269–286

[44] Dixon SJ, Lemberg KM, Lamprecht MR, Skouta R, Zaitsev EM, et al. 2012. Ferroptosis: an iron-dependent form of nonapoptotic cell death. *Cell* 149:1060–1072

[45] Cruz-Gregorio A, Aranda-Rivera AK. 2023. Quercetin and ferroptosis. *Life* 13:1730

[46] Wang Y, Branicky R, Noë A, Hekimi S. 2018. Superoxide dismutases: dual roles in controlling ROS damage and regulating ROS signaling. *The Journal of Cell Biology* 217:1915–1928

[47] Su L, Zhang J, Gomez H, Kellum JA, Peng Z. 2023. Mitochondria ROS and mitophagy in acute kidney injury. *Autophagy* 19:401–414

[48] Lu S, Wang XZ, He C, Wang L, Liang SP, et al. 2021. ATF3 contributes to brucine-triggered glioma cell ferroptosis via promotion of hydrogen peroxide and iron. *Acta Pharmacologica Sinica* 42:1690–1702

[49] Okazaki S, Umene K, Yamasaki J, Suina K, Otsuki Y, et al. 2019. Glutaminolysis-related genes determine sensitivity to xCT-targeted therapy in head and neck squamous cell carcinoma. *Cancer Science* 110:3453–3463

[50] Seiler A, Schneider M, Förster H, Roth S, Wirth EK, et al. 2008. Glutathione peroxidase 4 senses and translates oxidative stress into 12/15-lipoxygenase dependent- and AIF-mediated cell death. *Cell Metabolism* 8:237–248

[51] Chen X, Yu C, Kang R, Kroemer G, Tang D. 2021. Cellular degradation systems in ferroptosis. *Cell Death & Differentiation* 28:1135–1148

[52] Klaassen CD, Reisman SA. 2010. Nrf2 the rescue: effects of the antioxidative/electrophilic response on the liver. *Toxicology and Applied Pharmacology* 244:57–65

[53] Yang WH, Lin CC, Wu J, Chao PY, Chen K, et al. 2021. The hippo pathway effector YAP promotes ferroptosis via the E3 ligase SKP2. *Molecular Cancer Research* 19:1005–1014

[54] Doll S, Proneth B, Tyurina YY, Panzilius E, Kobayashi S, et al. 2017. ACSL4 dictates ferroptosis sensitivity by shaping cellular lipid composition. *Nature Chemical Biology* 13:91–98

[55] Lei G, Mao C, Yan Y, Zhuang L, Gan B. 2021. Ferroptosis, radiotherapy, and combination therapeutic strategies. *Protein & Cell* 12:836–857

[56] Conrad M, Pratt DA. 2019. The chemical basis of ferroptosis. *Nature Chemical Biology* 15:1137–1147

[57] Xue P, Zhang J, Wang Z, Wu L, Tang J, et al. 2025. Arachidonic acid induces ferroptosis in hepatocellular carcinoma via the SIRT5-ACSL4/

LPCAT3/ALOX15 axis, leading to lipid peroxidation and mitochondrial dysfunction. *Phytomedicine* 148:157450

[58] Zhou X, Xu S, Zhang Z, Tang M, Meng Z, et al. 2024. Gouqi-derived nanovesicles (GqDNVs) inhibited dexamethasone-induced muscle atrophy associating with AMPK/SIRT1/PGC1α signaling pathway. *Journal of Nanobiotechnology* 22:276

[59] Yang J, Yun X, Zheng W, Zhang H, Yan Z, et al. 2025. Nanoscale engineered exosomes for dual delivery of Sirtuin3 and insulin to ignite mitochondrial recovery in myocardial ischemia-reperfusion. *Journal of Nanobiotechnology* 23:439

[60] Liu J, Ren Z, Yang L, Zhu L, Li Y, et al. 2022. The NSUN5-FTH1/FTL pathway mediates ferroptosis in bone marrow-derived mesenchymal stem cells. *Cell Death Discovery* 8:99

[61] Li D, Lu X, Xu G, Liu S, Gong Z, et al. 2023. Dihydroorotate dehydrogenase regulates ferroptosis in neurons after spinal cord injury via the P53-ALOX15 signaling pathway. *CNS Neuroscience & Therapeutics* 29:1923–1939

[62] Ren X, Wen Y, Yuan M, Li C, Zhang J, et al. 2024. Cerebroprotein hydrolysate-I ameliorates cognitive dysfunction in APP/PS1 mice by inhibiting ferroptosis via the p53/SAT1/ALOX15 signalling pathway. *European Journal of Pharmacology* 979:176820